ALMA MEMO 390

Radio Interferometer Array Point Spread Functions

II. Evaluation and Optimization

David Woody[1]

***Abstract*—The PSF of several sample arrays, including pseudo-random and circular arrays, are evaluated. The distribution of sidelobes is shown to closely follow the theoretical distribution derived in the companion paper [1]. An optimization procedure is developed that produces configurations with peak sidelobes close to the expected limit given in [1] and with a smooth progression from small peaks near the center of the PSF and the largest peaks at the edge of the primary beam. Plotting the peak sidelobe as a function of the radial distance from the center of the PSF is shown to be very useful for evaluating the PSF. The optimized arrays provide a benchmark against which other configurations can be compared.**

I. Introduction

Evaluating the merits of different radio interferometer array configurations is a complex task involving many conflicting considerations. The Point Spread Function, PSF, provides a convenient and useful measure of the imaging capability of an array. A simple Fourier Transform of the visibility data gives an image that is the true sky brightness convolved with the PSF and the PSF sidelobes are a good measure of the imaging artifacts that a sophisticated imaging algorithm must correct or remove. This paper investigates the PSF for three very different arrays and compares the distribution of sidelobe peaks to the theoretical predictions of the companion paper [1]. Section II describes the three arrays of 64 or 65 antennas and presents the evaluation of their PSF's including plots of the peak sidelobe as a function of radial distance from the center of the PSF. These plots provide a very useful and easy to interpret visualization of the salient features of the PSF. The PSF are presented for configurations in which the FWHM of the PSF is $1/128^{th}$ of the primary beam, i.e. a magnification of 128.

A configuration optimization algorithm that minimizes peak sidelobes is described in section III. This algorithm follows the approach developed by Kogan [2]. The algorithm is applied to the arrays from section II and the results are presented.

The optimization procedure can be sequentially applied starting with the near sidelobes and progressing out to the farthest sidelobes. Section IV describes this procedure and applies it to the same three arrays. It is shown that the near sidelobes can be decreased significantly while still achieving the same low sidelobe limit for the far sidelobes. This should be very useful in imaging small regions within the primary beam where confusion or artifacts from distant sources is not a problem.

A further refinement is applied in section V where the goal is not to minimize the sidelobes but to come as close as possible to a desired average sidelobe level. Using this technique it is possible to produce PSF beams with sharp central beams together with a broad low level plateau that is positive even when the single dish or zero UV is not included. The resulting optimized configurations have sufficient short spacings to avoid resolving out modest sized sources, even in the simple Fourier Transform of the raw visibility data. Thus the short spacing requirement can be quantitatively cast in terms of the large object response of the PSF.

Section VI compares the statistical properties of the PSF for all of the arrays before and after optimization to the predictions from ref. [1]. The agreement is excellent for the pseudo-random array and even the other arrays are consistent with the predictions. After optimization all arrays evolve to look like pseudo-random arrays including matching the predicted statistical distribution and maximum sidelobe amplitude.

Practical considerations such as reuse of pads between configurations and the length of connecting roads are discussed in section VII. A summary and conclusion are given in section VIII.

II. Initial configurations

Three antenna configurations will be investigated in this section; a) a five-fold symmetric circular array of 65 antennas [3], b) a pseudo-random configuration of 64 antennas with a cosine squared bell shaped distribution, and c) an array of 64 antennas systematically placed to yield a cosine squared bell shaped distribution. The antenna positions for these arrays are shown in fig. 1. The widths of the three distributions have been scaled to give the same synthesized beam. A configuration of antennas of diameter *D* and a nominal magnification of *mag* is obtained by scaling the antenna positions by *mag*D*.

August, 2001

[1]Owens Valley Radio Observatory, California Institute of Technology, Big Pine, CA 93513, USA

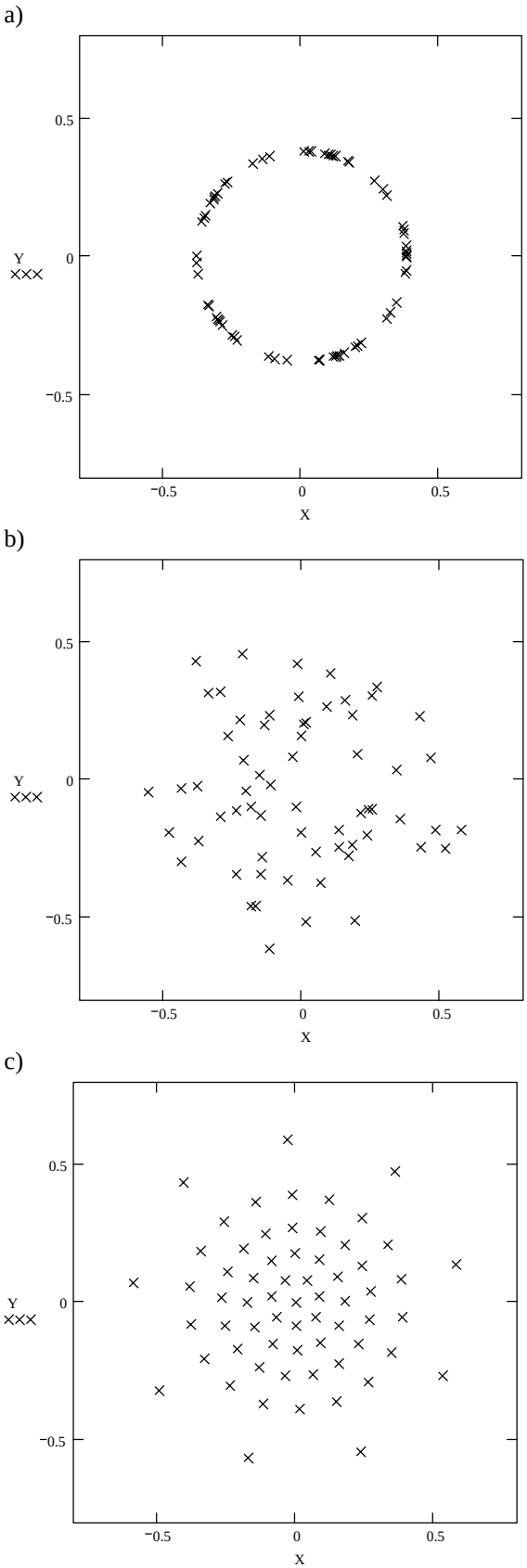

Fig. 1. Initial array configurations.

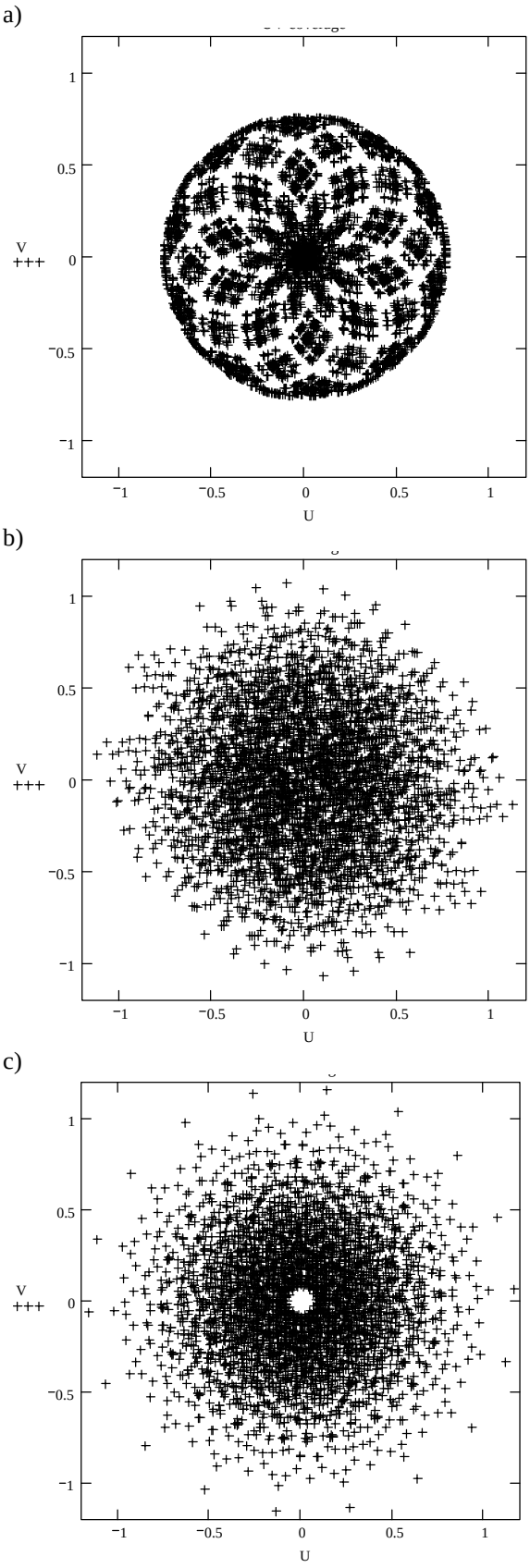

Fig. 2. UV snapshot coverage.

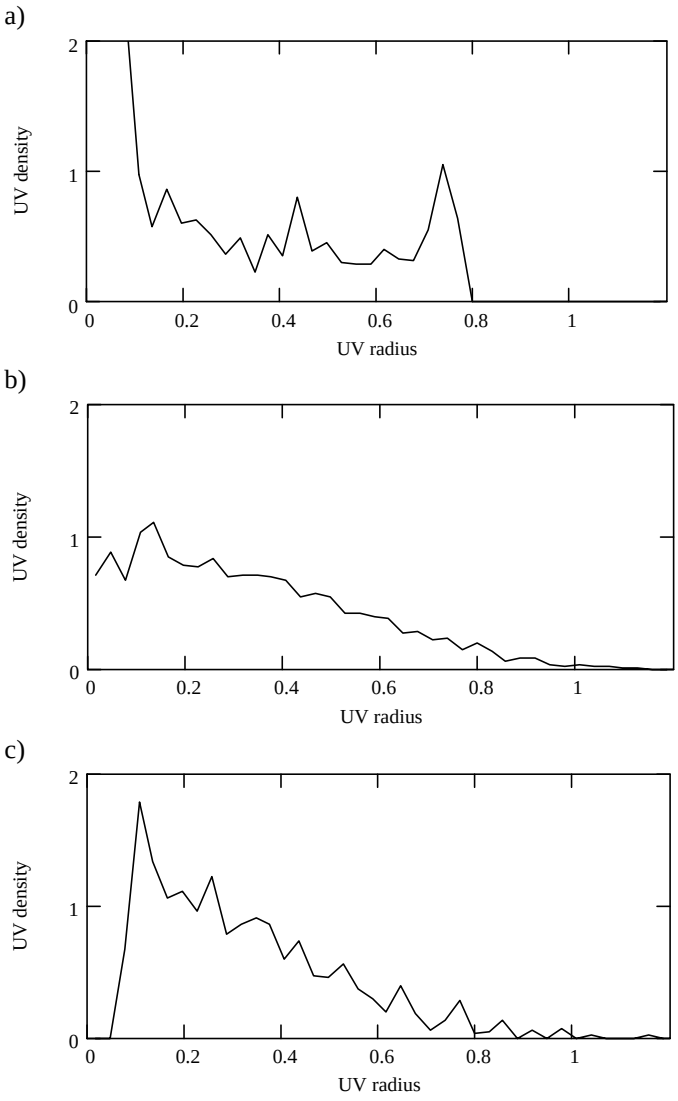

Fig. 3. UV sampling density vs. baseline length.

The circular array is based upon maximizing the magnification while maintaining nearly complete coverage. This configuration achieves nearly complete coverage at a magnification of ~190 for 2.5 hour long tracks. For the smaller magnification of 128 used here, the closest antennas have been shifted to ensure a separation greater 1.5 times the antenna diameter.

The snapshot UV coverage is shown in fig. 2 for the three configurations. The radial UV distribution is plotted in fig. 3. The circular array shows the characteristic peaking of the UV sampling at the longest and shortest baseline lengths while the bell shaped antenna distributions give a centrally condensed UV distribution. Note that while the pseudo-random configuration produced a reasonable number of short baselines, the systematic configuration lacks very short baselines.

The PSFs for these configurations operating at a magnification of 128 are shown in fig. 4. These plots of the PSF include effect of the primary beam appropriate for a

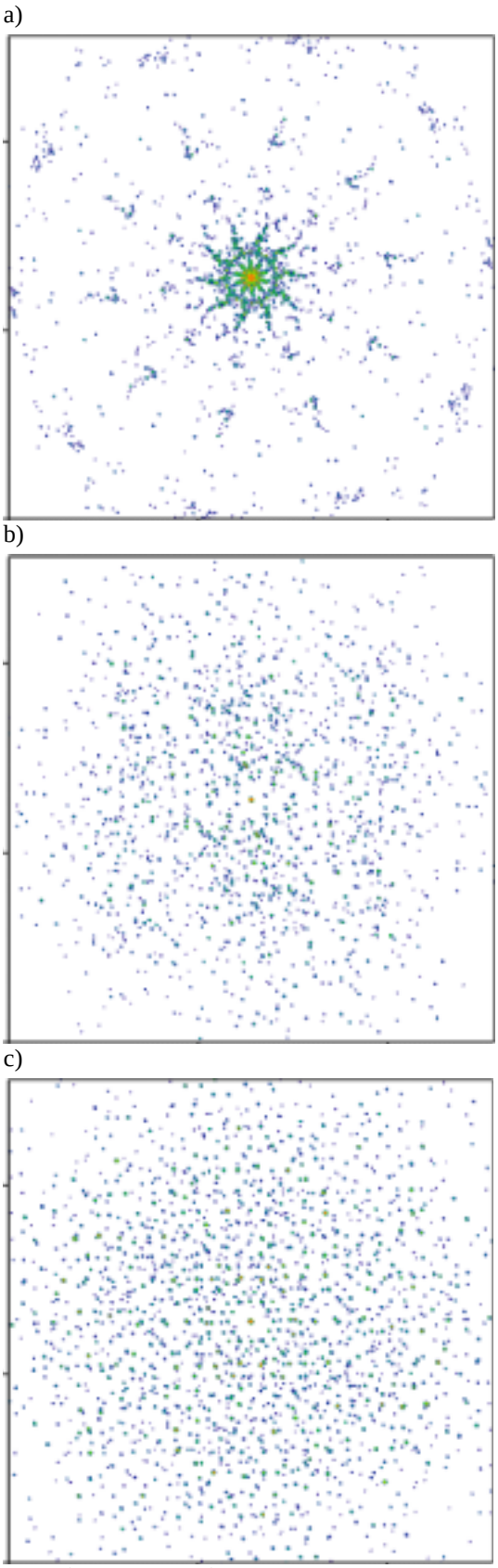

Fig. 4. PSF for the three configurations. The color scale is logarithmic spanning 5 to 15%.

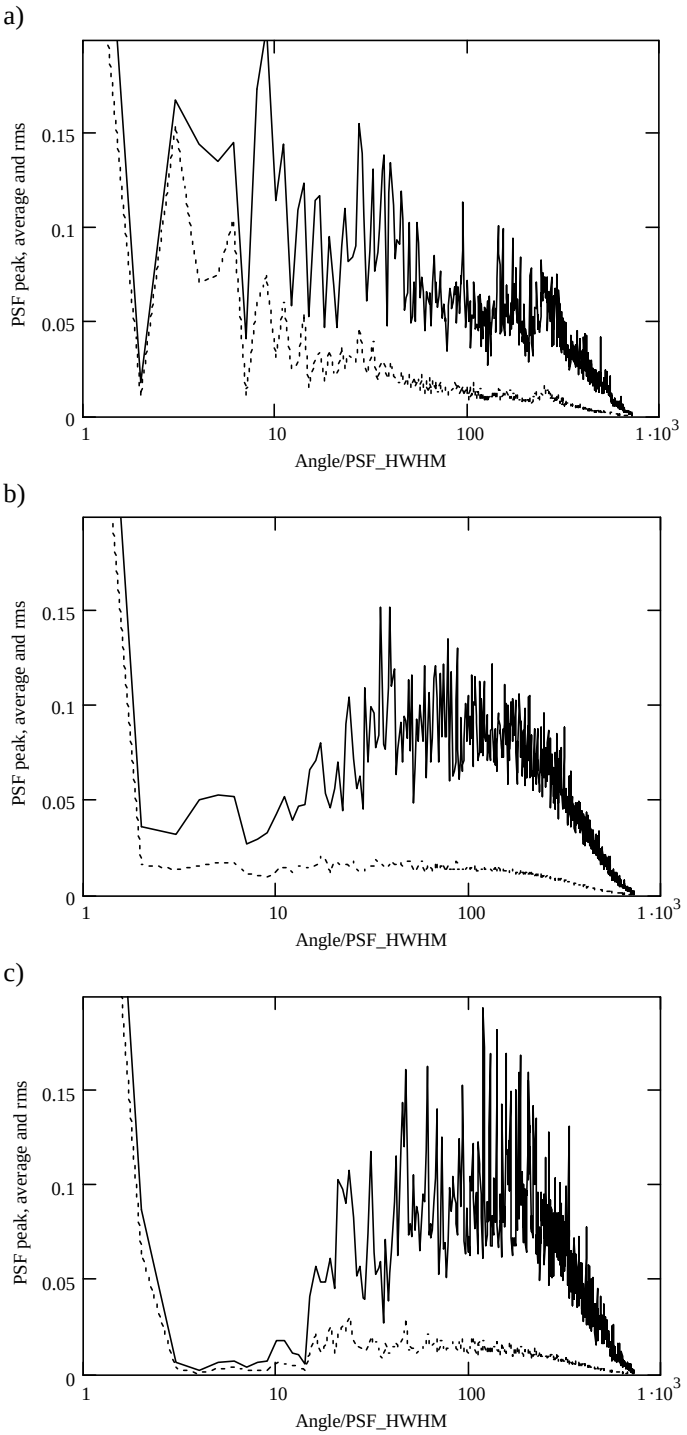

Fig. 5. Plot of the peak sidelobes of the PSF as a function of radial distance from the center of the beam (solid line). The dotted line is the azimuthal average of the PSF.

source at the field center, which limits the extent of the sidelobes. The regular structure in the circular array produces obvious prominent features in the PSF. Although the PSF for the circular array is distinctly different from the other two arrays, it is hard to distinguish the two bell shape configurations and particularly hard to make any quantitative statements about the sidelobes. A convenient method for evaluating the PSF is to plot the amplitude of largest peak in an azimuthal ring as a function of the ring radius as shown in fig. 5. The magnitude of the largest sidelobes and their distance from the center of the PSF are easily determined from these graphs. The large near sidelobes from the circular array are very apparent. The random arrays with a bell shaped distribution have low near sidelobes increasing away from the beam center. Notably, the near sidelobe peaks for the systematic cosine squared configuration c are less than the 1/(N-1)=1.6% contributed by the single antenna measurements [4]. Hence without the zero spacing UV data, there would be a significant negative bowl in the PSF extending out to ~10 times the HWHM.

The azimuthal average of the PSF is also plotted in fig. 5. This is indicative of the sidelobes that might be expected for long 12 hour tracks, although the actual sidelobes will depend upon the latitude of the array, it's elongation and the declination of the source.

III. Optimization

Reducing the largest sidelobes of the PSF improves the dynamic range in the images produced by an array. Kogan has developed an optimization routine that minimizes the sidelobes over selected radial and azimuthal ranges [2]. Boone has also developed an optimization algorithm that minimizes the deviation between the UV distribution and a target UV distribution [5]. This will also have the effect of minimizing the sidelobes.

The approach used here is similar to that of Kogan [2]. After identifying the largest PSF sidelobe, an antenna is selected at random for repositioning. As with Kogan's algorithm the derivative of the PSF at the peak with respect to the antenna's location is found using equ. 2 in ref. [1]. This derivative is used to determined the direction to move the antenna to decrease the sidelobe peak and the antenna is moved a small step in this direction. The PSF is recalculated and the largest sidelobe is found. If new the peak sidelobe is smaller than previous peak, the move is kept and the process repeated. If the new peak is larger, the antenna is returned to its original position and removed from the random selection pool and another antenna is selected at random. A successful move puts all antennas back into the selection pool. This proceeds until you reach a point where all antennas have been tried with no success, at which time the step size is decreased and the process started again. This procedure is repeated until you run out of computer time or the step size reaches a predetermined minimum size.

The algorithm does not necessarily find the global optimum but it can find several different local minima from the same starting configuration. The random sequence of antennas selected for repositioning means that the optimization path is not unique and the final configurations will differ slightly for each pass through the procedure.

The step sizes are typically smaller than an antenna diameter and gridding the antenna positions to use an FFT would require an exceedingly small cell size and hence a very large data array. A DFT is actually more efficient since there

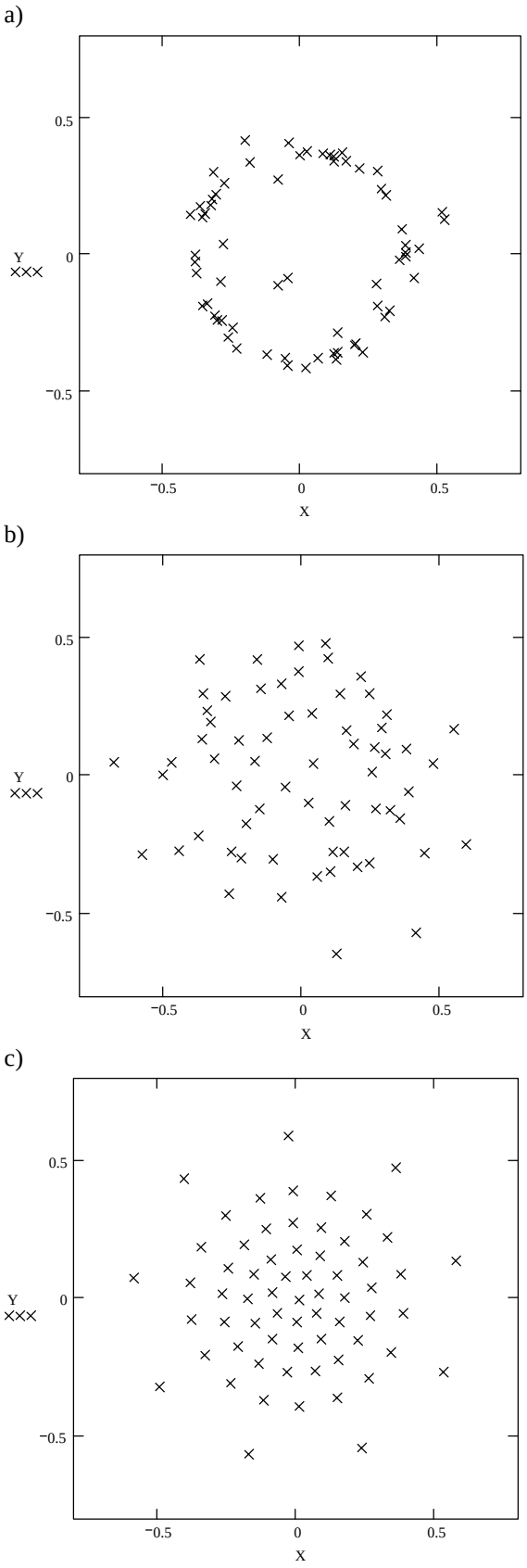

Fig. 6. Optimized array configurations starting from the same configurations as shown in fig. 1.

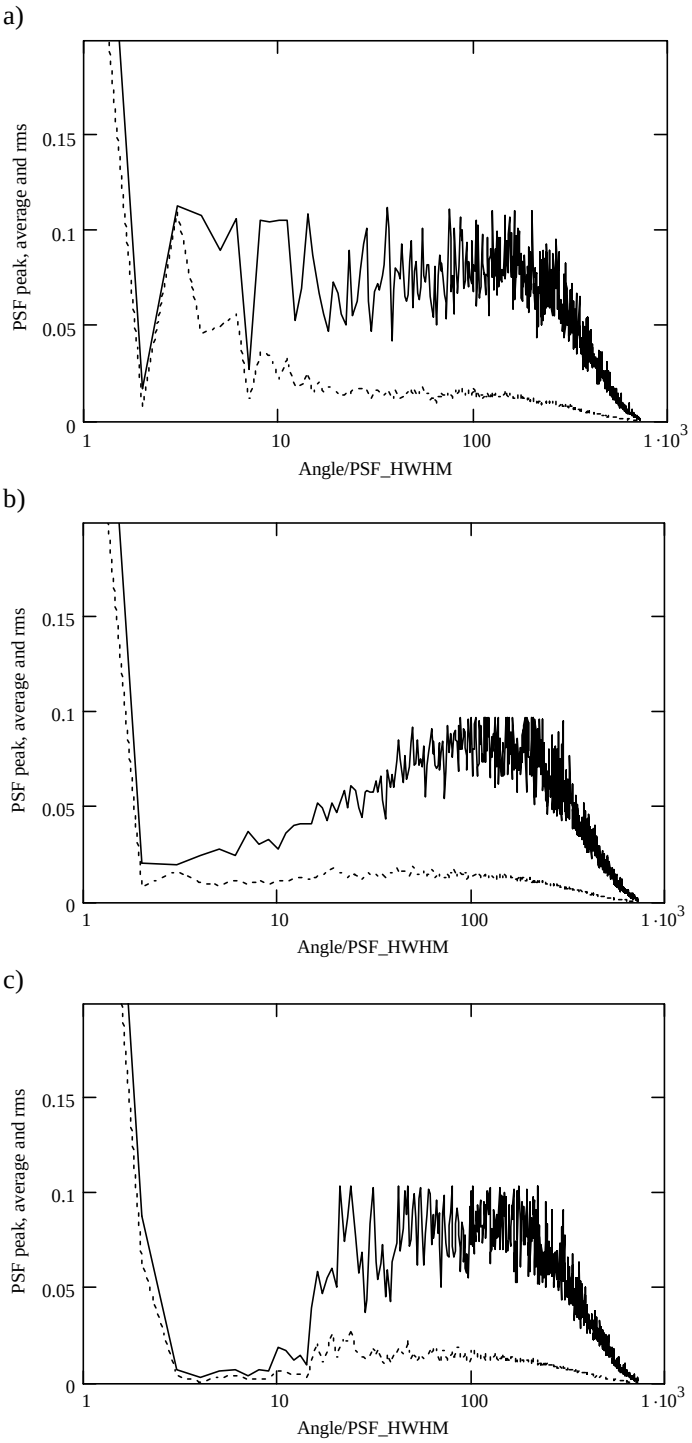

Fig. 7. Radial plot of the peak sidelobes after optimizing the configurations from fig. 1 (solid line). The dotted line is the azimuthal average of the PSF.

are only N=64 terms in the summation for each point in the PSF.

Figure 6 shows the three new configurations resulting from applying this optimization procedure to the arrays evaluated in section II. The magnitude of the alterations from the initial configuration depends upon the distance of the largest sidelobes from the center of the PSF. Reducing the near sidelobes from the circular configuration requires larger motions than reducing the far sidelobes in the systematic

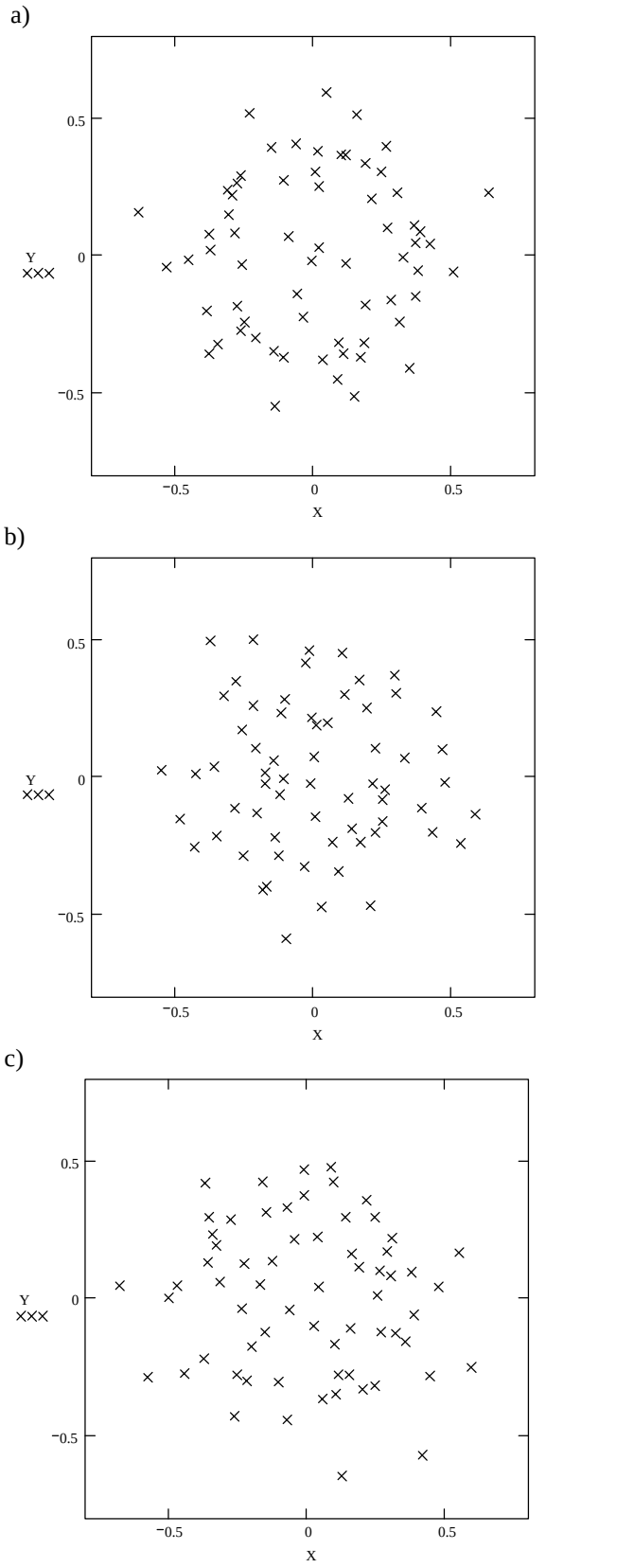

Fig. 8. Sequentially optimized array configurations starting from the same configurations as shown in fig. 1.

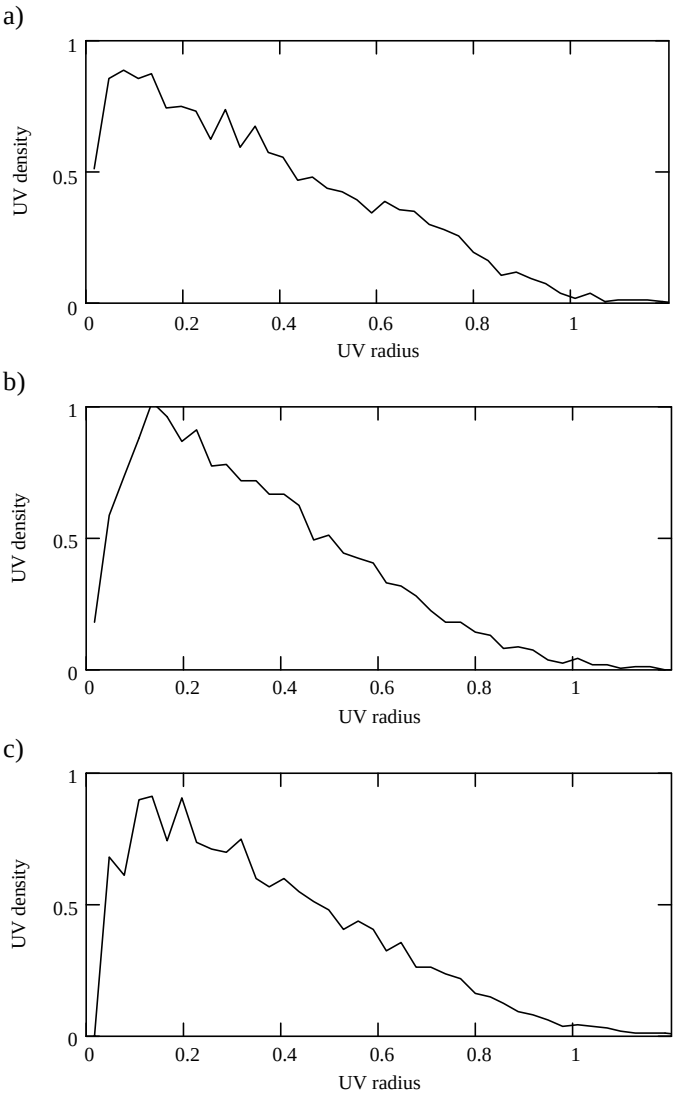

Fig. 9. UV sampling density vs. baseline length after sequentially optimizing the circular, pseudo-random and systematic arrays in fig. 1.

array. The antenna shifts in the systematic configuration are barely discernable. The radial plots of the sidelobe peaks in fig. 7 show that the algorithm was very effective in decreasing the largest peaks to a common lower value.

IV. Sequential Optimization

The sidelobes at different distances from the center of the PSF correspond to the distribution of the antennas on different size scales. Hence the sidelobes at widely different distances are somewhat independent. In particular, the small motions that can significantly affect the far sidelobes have almost no effect on the near sidelobes. This leads to a modified optimization algorithm that progressively works on minimizing the sidelobes starting from the nearest ones and proceeding out to the farthest sidelobes.

This has been implemented here by sequentially minimizing the peak sidelobes within 8 to 128 times the HWHM of the PSF in octave steps. The resulting

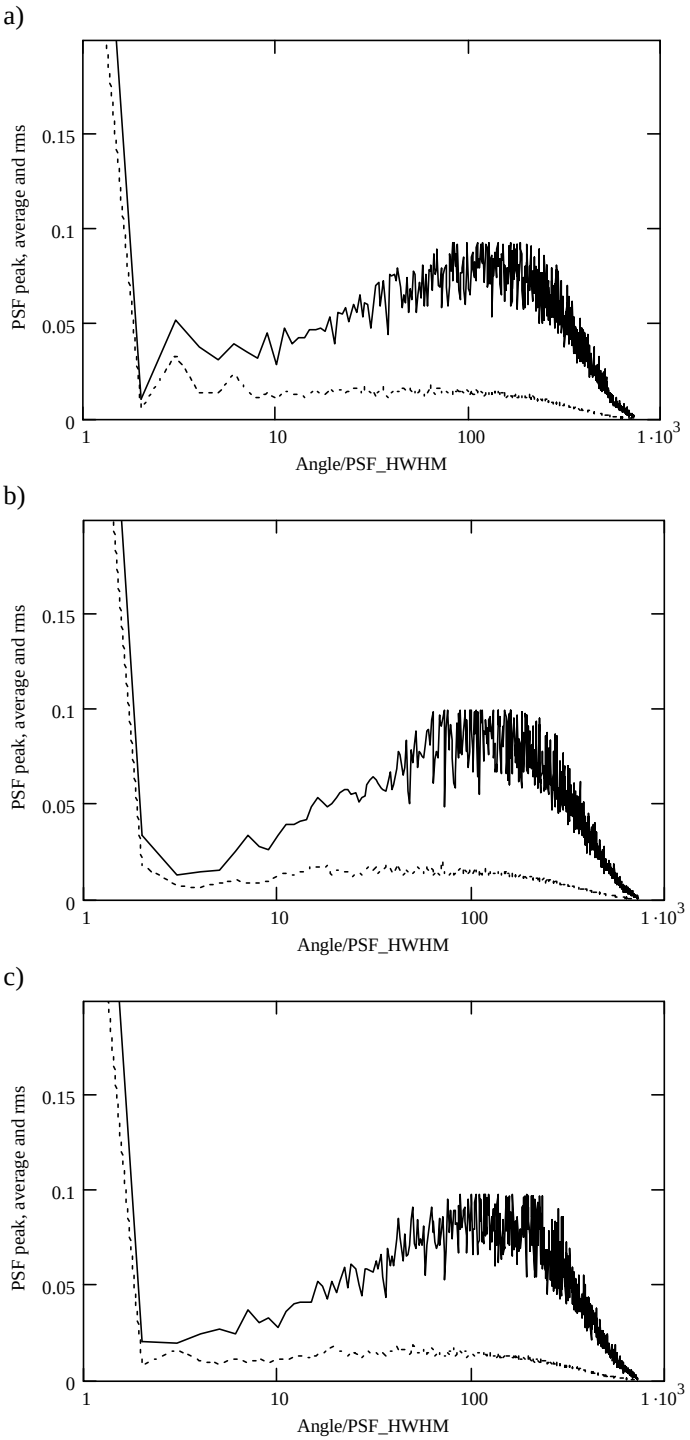

Fig. 10. Radial plot of the peak sidelobes after sequentially optimizing the configurations from fig. 1 (solid line). The dotted line is the azimuthal average of the PSF.

configurations are displayed in fig. 8 and the radial UV sample density in shown in fig. 9. This more extensive optimization procedure has transformed all three configuration into looking more like pseudo-random arrays, although the under lying circle is still apparent in fig. 8 panel a), with very similar UV distributions. Figure 10 shows the radial plots of the PSF peaks. The remnant of the circle still leaves noticeable near sidelobes. The nearest sidelobes are difficult to optimize because of the large shift in telescope positions required.

V. Generalized Optimization

The initial systematic configuration and the single optimization of the configuration have very low near sidelobes but almost no short baselines. Hence, in the absence of the single dish data even slightly extended sources will be resolved out. This is a common problem and it is often stated that a good sampling of short baseline lines is required to yield reliable images. Excluding the single dish data from the calculation lowers the PSF by 1/(N-1)=1.6% for a 64 antenna array [4] and the low near sidelobe actually become negative. In the interest of imaging extended objects without requiring single dish data, the PSF should be positive or at least the azimuthal average greater than zero out as far as possible.

The optimization routine was modified to evolve the array to match the PSF to a predetermined value and not just minimize the peaks. In this case the absolute value of the difference between the PSF and the predetermined value was used to determine the offset position of the peak or minimum that needed to be reduced. The rest of the algorithm remained the same, but with proper account of whether an antenna needed to be moved to increase or decrease the PSF at the offset position.

This was applied sequentially as described in the previous section to the systematic array using a predetermined PSF value of 2.5%. Figure 11 shows the resulting configuration and the UV sample density is plotted in fig. 12. This optimization procedure has produced a small ring of antennas near the center of the array and the UV distribution is nearly Gaussian with a small excess at the shortest spacings.

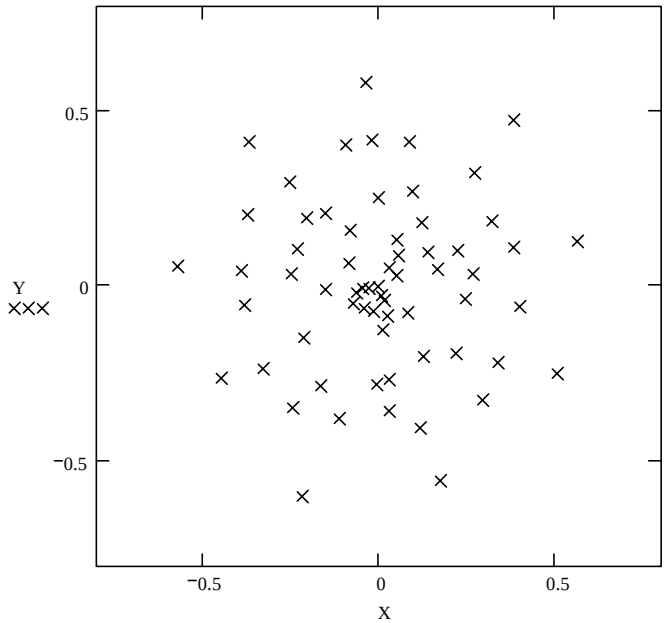

Fig. 11. Configuration after optimizing the systematic array for a PSF of 2.5%.

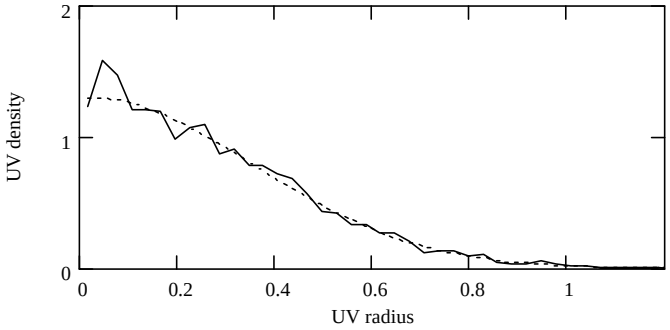

Fig. 12. Radial plot of UV sample density for the configuration shown in fig. 11 (solid line). The dotted line is a best fit Gaussian distribution.

The PSF is shown in fig. 13 and radial plot of the sidelobe peaks is displayed in fig. 14. The target value of 2.5% is 0.9% above the contribution of the single dish data so that in the absence of this data the PSF will be positive and well behaved, at least near the center. Eventually the PSF has to become negative because without the U=V=0 data, the PSF must average to zero across the primary beam. The peak and average are very close out to ten times the HWHM and the peak of the PSF sits atop a reasonably clean plateau in this region as can be seen in the expanded view of the PSF shown in fig. 15.

VI. Statistics

Several statistical properties for the sidelobes of the PSF of pseudo-random arrays are derived in ref. [1]. The standard deviation of the sidelobes for a sparse array is predicted to be ~1/N, where N is the number of antennas. The standard deviations of the sidelobes for all of the arrays evaluated in this paper, including the circular and systematic configurations, are within 10% of this value.

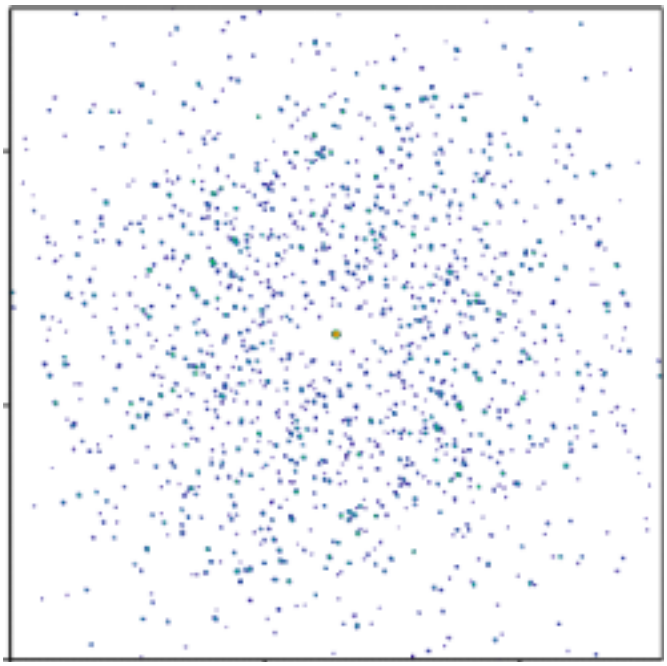

Fig. 13. PSF for the configuration in fig. 11. The color scale is logarithmic spanning 5 to 15%.PSF for

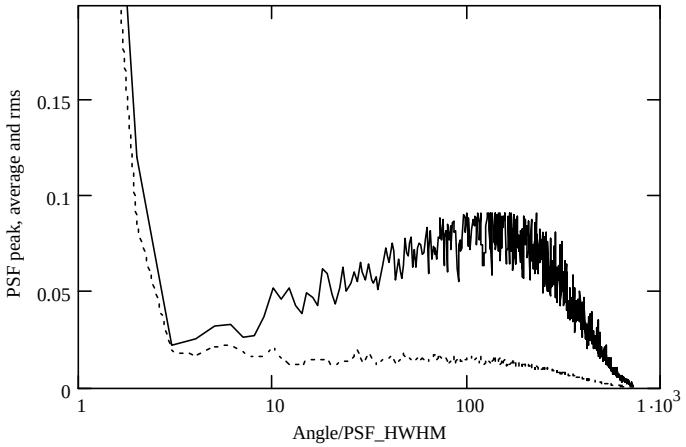

Fig. 14. Radial plot of peak sidelobes for the configuration in fig. 11 (solid line). The dotted line is the azimuthal average of the PSF.

Reference [1] also predicts that the distribution of PSF sidelobe amplitudes for a pseudo-random array will follow

$$g(s) = N \exp(-Ns), \quad (1)$$

where s is the sidelobe amplitude. This can be tested by comparing the histograms of PSF sidelobes for the various arrays evaluated here to equ. 1. This comparison is shown the initial three arrays from section II in fig. 16. The histograms and theory have been normalized to give unity when integrated over all sidelobe amplitudes. The pseudo-random array closely matches the predicted distribution. The other arrays also match the calculated distribution for small amplitudes but have an excess of large sidelobes. This is especially apparent for the circular array with its large near sidelobes.

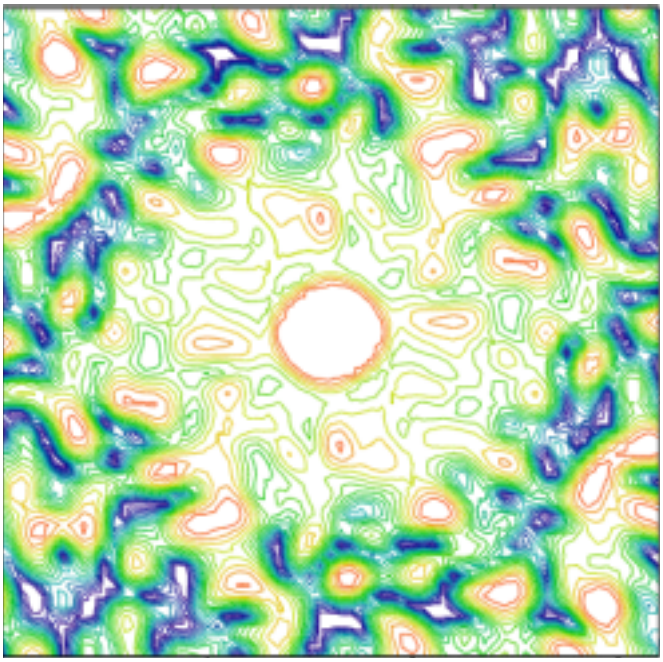

Fig. 15. PSF for the configuration in fig. 11 expanded to show the central core out to 16 times the HWHM. The color scale is logarithmic spanning 0.1 to 5% with low color intensity at the target value of 2.5%.

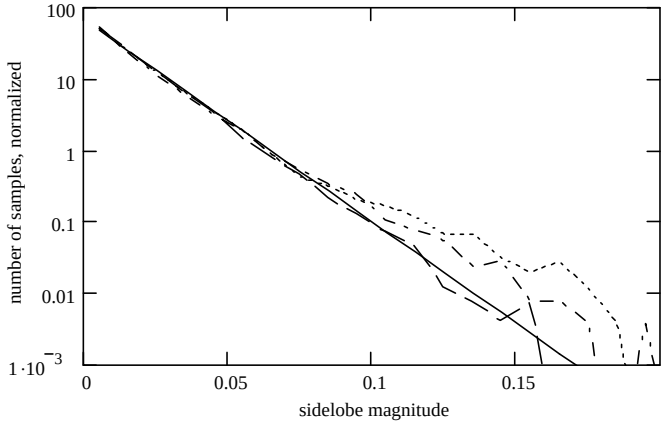

Fig. 16. Histograms of the PSF sidelobe amplitudes for the initial circular array (dotted), pseudo-random (dashed) and systematic (dot-dash). The solid line is the theoretical distribution for pseudo-random configurations.

The distributions of sidelobe amplitudes for all three configurations closely follow the prediction for pseudo-random arrays after they have been optimized. Figures 17 and 18 show the PSF amplitude histograms for single and sequential optimization procedures respectively while fig. 19 shows the amplitude histogram for the configuration optimized for a PSF value of 2.5% in the previous section.

The theory in ref. [1] also predicts the amplitude of the largest PSF sidelobe before and after optimization. Before optimization the maximum sidelobe is expected to be

$$s_{\max} \approx \frac{2}{N}\ln(mag), \tag{2}$$

where *mag* is the magnification of the array, i.e. the ratio of the primary beam to the synthesized beam. Figure 20 plots the amplitude of the largest sidelobe for several different arrays, including the three evaluated in section II, when scaled to produce different magnifications. After optimization the largest sidelobe is predicted to be

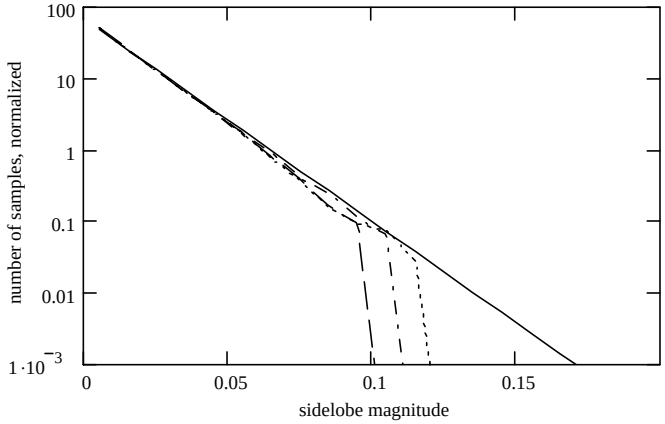

Fig. 17. Histograms of PSF sidelobe amplitudes after optimization of the circular array (dotted), pseudo-random (dashed) and systematic (dot-dash). The solid line is the theoretical distribution for pseudo-random configurations.

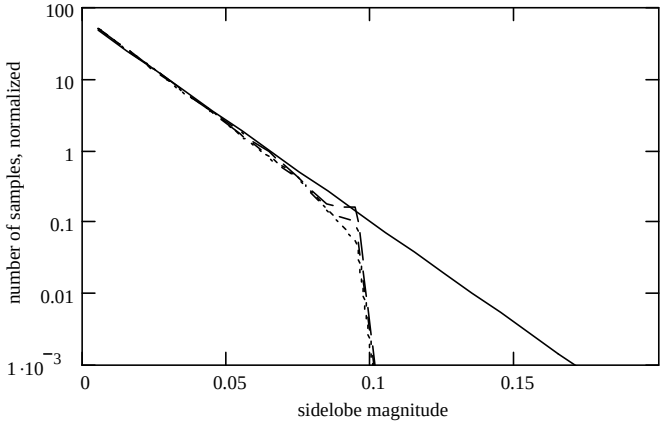

Fig. 18. Histograms of the PSF sidelobe amplitudes after sequential optimization of the circular array (dotted), pseudo-random (dashed) and systematic (dot-dash). The solid line is the theoretical distribution for pseudo-random configurations.

$$s_{\max,opt} \approx \frac{1}{N}\left[2\ln(mag) - \ln(N)\right]. \tag{3}$$

The largest sidelobes for the optimized versions of the arrays are also plotted in fig. 20. It is seen that the pseudo-random arrays agree reasonably well with the predictions for the before optimization peak sidelobe and that all of the arrays follow the same trend line after optimization, but exceed the predictions at low magnification. The prediction in equ. 3 clearly has a problem at low magnification since it predicts negative maximum peaks for $mag^2 < N$. This can be partially remedied by adding the average sidelobe given by 1/(N-1) to equ. 3 giving

$$s_{\max,opt} \approx \frac{1}{N}\left[1 + 2\ln(mag) - \ln(N)\right]. \tag{4}$$

This gives somewhat better agreement with the results for optimized arrays.

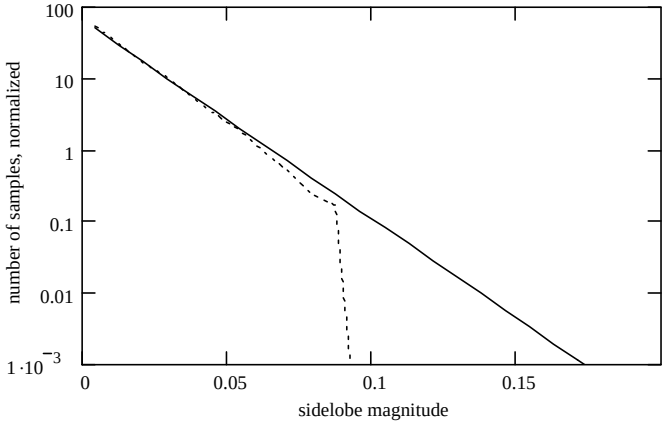

Fig. 19. Histogram of sidelobe amplitudes for the PSF in fig 13 (dotted line). The solid line is the theoretical distribution for pseudo-random configurations.

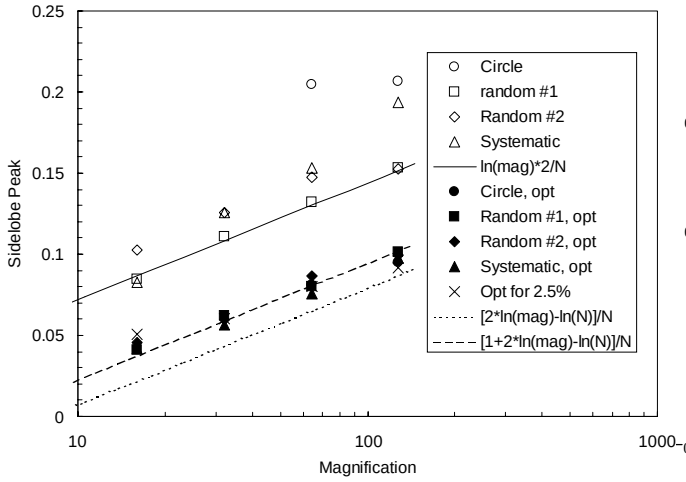

Fig. 20. Largest sidelobe for various configurations as a function of their magnification.

VII. Other Considerations

Most radio interferometers have several different configurations for the antennas corresponding to different source declination ranges or magnifications and images often involve combining UV data from several configurations. It may be desirable to have some of the antenna locations in common between configurations, although if too many locations are in common, you do not obtain as much unique UV data.

The pseudo-random and various optimized arrays presented here are well suited to sharing antenna locations between configuration since they are centrally condensed, i.e. all configurations will have positions near the center of the array that can be used by several or even all of the configurations. The lowest magnification configuration would be fully optimized. Then a number of the stations would be randomly selected for use in the next larger magnification configuration and the configuration would be optimized with these stations held fixed. This would proceed out to the largest magnification configuration. It only needs to be decided what fraction of the stations to reuse. Freezing 10 to 20% of the stations will have only a small effect on the maximum sidelobe.

Geographic or other constraints can also be handled in the optimization routine by not allowing an antenna to be moved into a forbidden region. The effect of such constraints will depend upon their extent, but because there is no grand design for pseudo-random or optimized arrays they should be as tolerant of the constraints as any other configuration.

Roads can be a significant cost for the largest configurations, so array configurations requiring excessively long roads should be avoided. But it turns out that almost any array of a large number of antennas distributed over a plane will require a similar length of road. Circular or thin ring arrays and simple star arrays can have shorter road lengths but they produce PSFs with significantly larger sidelobes. Figure 21 shows a computer generated road for the array in fig. 11. The length of this road is 4.9 times the longest baseline and hence is only 56% longer than a circle encompassing the array.

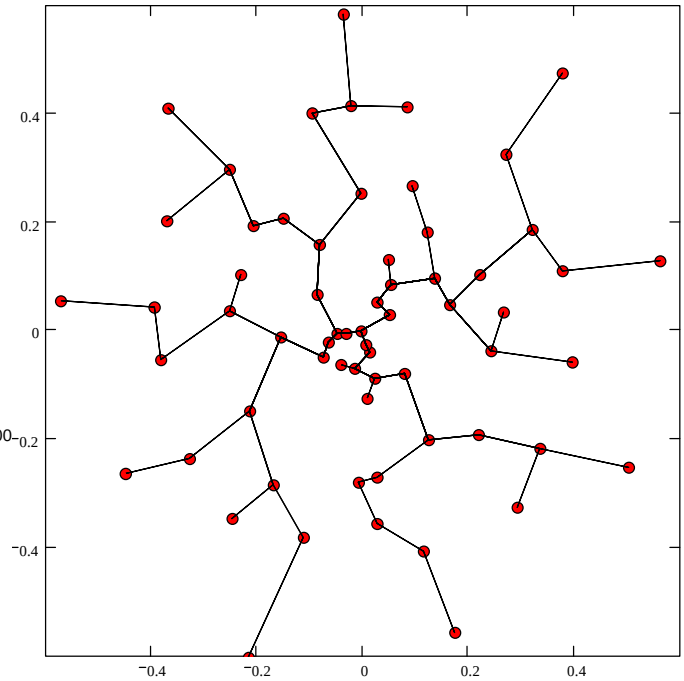

Fig. 21. Road placement for the optimized array from section V.

The ALMA project is considering adding an array of smaller antennas to fill in the sparsely sampled short spacings. The area inside the circular cluster of antenna near the center of the array is a natural location for this small array.

VIII. Summary and Conclusion

Several quite different array configurations have been evaluated, including circular, pseudo-random and configurations with the antennas systematically placed to yield a cosine squared distribution. The UV distribution and PSF functions reveal the major differences between these configurations. The statistical properties for the pseudo-random array closely matched the predictions from ref. [1], as did the standard deviation and distribution of sidelobe amplitudes at small amplitude for the other arrays. The PSF of the other arrays had an excess number of large sidelobes. The radial plot of the maximum sidelobes provides a clear and convenient method for evaluating the PSF.

An optimization procedure was described that was very effective in reducing the peak sidelobes of all three initial configurations to close to the predicted limit. It was shown that the optimization could be applied sequentially starting at the near sidelobes and proceeding to the far sidelobes. This produces PSFs whose peak sidelobes increase gradually from low values near the center of the synthesized beam out to the far sidelobes with the maximum sidelobe still at the predicted limit. After sequential optimization, all of the arrays looked essentially like pseudo-random arrays with bell shaped UV distributions. An additional modification of the routine was used to produce a configuration with a PSF consisting of a

sharp central synthesized beam sitting on top of a low extended plateau. The resulting UV distribution was Gaussian plus an excess of short baselines. These latter configurations should provide excellent imaging capability both in terms of high dynamic range and fidelity with a minimum reliance on the single antenna data for mapping extended sources.

Designing an array configuration involves many different conflicting requirements and there is no single global optimum, but the evaluation and optimization procedures described here, together with the statistical properties derived in ref. [1], are useful for comparing different configurations and determining if they can be improved significantly.

REFERENCES

[1] D. Woody, “Radio Interferometer Array Point Spread Functions I. Theory and Statistics," ALMA memo #?, August 2001.

[2] L. Kogan, “Optimizing a Large Array Configuration to Minimize the Sidelobe,” IEEE Trans. Antennas Propagat., vol. 48, pp. 1075-1078, July 2000.

[3] D. Woody, "Circular Array Configuration", ALMA memo 270, July 2000.

[4] L. Kogan, “Level of Negative Sidelobes in an Array Beam,” Pub. Astron. Soc. Pac. vol. 111, pp. 510-511, 1999.

[5] F. Boone, “Interferometric array design: antenna positions optimized for ideal distributions of visibilities,” Aston. & Astrophy, Feb. 2001.